Binder MIMO Channels

Bin Lee, John M. Cioffi, Kibeom Seong, Youngjae Kim, Mehdi Mohseni, and Mark H Brady

Department of Electrical Engineering

Stanford University

Stanford, CA, 94305

Email: {binlee, cioffi, kseong, youngjae, mmohseni, mhbrady}@stanford.edu

Abstract This paper introduces a multiple-input multiple-output (MIMO) channel model for characterization of a binder of multiple telephone lines. This model is based on multiconductor transmission line theory and uses parameters that can be obtained from electromagnetic theory or existing measured data. The model generates frequency-dependent matrix channel/binder transfer functions as a function of cable type, geometric line-spacing and twist-length parameters, and source-load configurations. The model allows extraction from the binder matrix of the magnitude and the phase of individual NEXT, FEXT, split-pair and phantom transfers. These individual crosstalk transfer functions are often found to be very sensitive to small imperfections. Examples of category 3 twisted-pair American telephone lines and "quad" telephone cables appear.

Index Terms— MIMO systems, Crosstalk, Multiconductor transmission lines, Twisted pair cables, Subscriber loops

I. INTRODUCTION

Twisted-pair telephone line modeling to date has largely been of an individual line's insertion loss and transfer function. Crosstalk between lines has been modeled in magnitude-only by averaged transfer functions that represent the summed effect of several crosstalkers. These models have served the DSL and 10/100/G Ethernet communities well. However, with new vectored and/or bonded DSL systems mitigating and possibly exploiting crosstalk between multiple lines [1]-[2], the models for the binder of twisted-pair need significant improvement. This paper introduces a model for multiple-input-multiple-output (MIMO) telephone lines that allows computation of both the magnitude and phase of all the possible energy transfers within a binder, be them direct line transfer functions or representing various types of crosstalk. The intent of the models is to enable more accurate and dependable characterization of the various MIMO methods that can be applied to binders of twisted-pairs to increase supported data rates, and in particular to model category 3 telephone lines' use to bandwidths of 100's of Megabits per second or possibly even a gigabit per second, while allowing 100m category 5e, 6, and 7 transmission of 10Gbps Ethernet data rates (i.e., 10GBT).

The focus of this work will be to extend the traditional and well-known RLCG [3] models for individual twisted pairs to the matrix **RLCG** models examined for general electromagnetic coupling by C. Paul in [4]. Parallels with the traditional scalar effects and well-known formulas are made throughout this paper. To this objective, this work focuses on the basic unit of a section of multiple-twisted-pair binder with N pairs or equivalently $2N$ wires. Such a binder has actually $2N-1$ differential couplings that are all modeled in this paper via this basic unit. Vectors of voltages and currents replace scalars as in Paul. This paper introduces the thought-provoking load and source matrices and the potential of matrix-matched loading, which is conceptually similar to the single-line case but greatly differs in implementation and result for MIMO binders. This paper also illustrates the proper extraction of individual NEXT, FEXT and other interesting transfers (like phantoms and split pairs) from the MIMO matrix model and leads to simple explanations of some observed effects in measured NEXT and FEXT heretofore significantly misunderstood.

The limitations of previous research justifies this additional work. Past transmission practice within binder cables was differential excitation of individual pairs. Thus, channel studies focused on characterizing wire pairs under differential excitations. These studies did not treat binder cables as MIMO channels. Nevertheless, previous research generated many interesting results and methods that prepare us for the binder MIMO model of this paper: particularly, methods on modeling twisting for twisted pair cables [5]-[6], on the importance of cable imperfections [7]-[8], and empirical power sum characterization [9]. This paper's proposed binder MIMO model extends previous twisting models from a single twisting rate per pair to a cable binder, and incorporates cable imperfections. It also uses empirical power-sum results to verify its predictions.

This paper is organized as follows: Section 2 introduces the modeling of $2N$ wires or N lines. Matrix RLCG models are used to characterize an incremental section, following Paul's more general treatment of this subject. Terminology is introduced that directly parallels well-known scalar RLCG models in heavy use. Section 2 also investigates the appropriate matrix sources and loads and their construction, definition, and relation to traditional N-independent differential excitations. An interesting result is that traditional scalar matched differential sourcing and loading corresponds to an unusual singular situation in the MIMO case that is not at all well-matched in the MIMO case. In fact, the singular "mismatch" in the traditional scalar-matching leads to the large frequency-dependent ripples that have been long observed in measured FEXT and NEXT results, but often not so directly explained previously. Section 2 then also lays a foundation for cascades of binder sections that not only allow modeling of traditional gauge changes and "bridged-taps" but also allow modeling of twisting and binder imperfections like twist-rate variation and pair-center-separation variation. Section 3 shows that perfect twisting indeed almost entirely eliminates any crosstalk and that imperfect twisting causes actual measured crosstalk to be several orders larger than what would be produced by perfect twisting. Section 3 also includes a few basic comparisons of actual measured characteristics and computed characteristics, providing a strong indication of the model's successful potential use in modeling of MIMO binder transmission. Section 4 concludes the paper.

II. BINDER MIMO CHANNEL

The goal of the binder MIMO channel model is to obtain channel characteristics for closely packed multi-conductor wires. Using MIMO theory, the channel response can be expressed as:

$$\mathbf{Y} = \mathbf{HX} + \mathbf{N} \quad \textbf{(1)}$$

where $\mathbf{X}$ is an input column vector, $\mathbf{Y}$ is an output column vector, and $\mathbf{N}$ denotes noise components including impulse noise, radio frequency noise and other background noises. The binder MIMO channel model provides a method to calculate $\mathbf{H}$ from system physical parameters. With $\mathbf{H}$, the direct line transfer function, NEXT and FEXT, which are commonly used under differential excitation, can be easily calculated.

The binder MIMO channel model uses two concepts: circuit theory and cable geometric modeling. The circuit theory is used to derive voltage-current input-output relation for a cable system. Such derivation requires per-unit-length circuit elements that will be provided by the cable geometric modeling. This section first presents the circuit theory for a binder MIMO channel, followed by a treatment of the cable geometric modeling.

A. Circuit Theory For Binder MIMO Channel

The circuit theory for binder MIMO channel is based on multiconductor transmission line (MTL) theory [4]. To apply the theory, a complete cable loop is treated as the cascade of many segments. Additionally, this approach elucidates that proper source or load matrices may be more appropriate at both ends of the cable if possible to implement. This subsection first applies MTL theory to a cable segment to obtain voltage-current input-output relations for such a segment; then, the binder MIMO transfer matrix for the system can be calculated for the given source-load configuration. A designer may then cascade sections, multiplying matrix transfers to generate the individual NEXT, FEXT and line transfer function for the entire binder under study. This subsection also includes a discussion of split-pair and phantom transfer functions. All these theories assume that certain matrix resistance, inductance, capacitance, and conductance values, **RLCG,** are known for each segment. Models for

these matrices to complete these theories appear at the end of this subsection. Methods to obtain **RLCG** for given geometry configuration are also included.

1) MTL Theory For a Cable Segment

In multiconductor transmission line theory, the small segment of cable shown in Fig. 1(a) can be characterized by matrix parameters **RLCG**. In the following discussions, to reduce the complexity of drawing and indexing, four conductor wires are to simplify illustration. All results and formula can be directly extended to more wires but are difficult to draw. For a four-wire cable, one wire can be selected as a common reference; then, input-output characteristics for the cable can be completely modeled using 3 voltages and 3 currents. To describe these transmission lines, 4 incremental resistances, 6 capacitances, 6 inductances, and 6 conductances are required. Fig. 1(a) shows the labeling and indexing of these circuit elements.

The input-output voltage and current relations for a cable segment can be characterized by a transfer matrix $\mathbf{\Phi}$ as in Fig. 2 and in the following formula:

$$\begin{bmatrix} \mathbf{V}(z+d,\omega) \\ \mathbf{I}(z+d,\omega) \end{bmatrix} = \mathbf{\Phi}(z,d,\omega) \begin{bmatrix} \mathbf{V}(z,\omega) \\ \mathbf{I}(z,\omega) \end{bmatrix} \quad \textbf{(2)}$$

$$\mathbf{\Phi}(z,d,\omega) = \begin{bmatrix} \mathbf{A}(z,d,\omega) & \mathbf{B}(z,d,\omega) \\ \mathbf{C}(z,d,\omega) & \mathbf{D}(z,d,\omega) \end{bmatrix} \quad \textbf{(3)}$$

where $\mathbf{V}(z)$ and $\mathbf{I}(z)$ are column vector, z is the starting position of the cable segment and d is the length of the segment under consideration. **A, B, C, D** are 3×3 matrices. The position and frequency dependence of **A, B, C, D**, **V, I** and $\mathbf{\Phi}$ are explicitly shown in these formulas. The position dependence becomes important when twisting (See Fig.1(b)) and cable imperfections are included in the model. In the rest of the paper, notation for explicit frequency dependence is dropped for convenience. Furthermore, without loss of generality, $z = 0$ is assumed.

In general**,** a cable segment can be described by a position-dependent transmission-line equation. In practical cable systems, **L, C,** and **G** are slowly varying with distance along the cable, thus a position-

independent transmission line equation can be used for each segment. For channel-modeling purposes, time-invariant transmission-line equations for each segment are:

$$-\frac{d\mathbf{V}}{dz} = (\mathbf{R} + j\omega\mathbf{L})\cdot\mathbf{I} = \mathbf{Z}\cdot\mathbf{I}$$
$$-\frac{d\mathbf{I}}{dz} = (\mathbf{G} + j\omega\mathbf{C})\cdot\mathbf{V} = \mathbf{Y}\cdot\mathbf{V} \qquad \textbf{(4)}$$

where $\boldsymbol{Z} = \boldsymbol{R} + j\omega\boldsymbol{L}$ is the symmetric **impedance per unit length matrix** and $\boldsymbol{Y} = \boldsymbol{G} + j\omega\boldsymbol{C}$ is the symmetric **admittance per unit length matrix.** The explicit matrix forms of **RLCG** are given in Fig.1(a). The input-output relation for voltage and current, as well as the $\boldsymbol{\Phi}$, can be solved for each segment by extending the well known two-port theory results ([10]-[11]):

$$\begin{bmatrix}\mathbf{V}(0)\\ \mathbf{I}(0)\end{bmatrix} = \begin{bmatrix}\cosh(\boldsymbol{\gamma}d) & \sinh(\boldsymbol{\gamma}d)\cdot\mathbf{Z}_0\\ \sinh(\boldsymbol{\gamma}^T d)\cdot\mathbf{Z}_0^{-1} & \cosh(\boldsymbol{\gamma}^T d)\end{bmatrix}\cdot\begin{bmatrix}\mathbf{V}(d)\\ \mathbf{I}(d)\end{bmatrix} = \boldsymbol{\Phi}(d)\cdot\begin{bmatrix}\mathbf{V}(d)\\ \mathbf{I}(d)\end{bmatrix} \qquad \textbf{(5)}$$

$$\boldsymbol{\Phi}(d) = \begin{bmatrix}\cosh(\boldsymbol{\gamma}d) & \sinh(\boldsymbol{\gamma}d)\cdot\mathbf{Z}_0\\ \sinh(\boldsymbol{\gamma}^T d)\cdot\mathbf{Z}_0^{-1} & \cosh(\boldsymbol{\gamma}^T d)\end{bmatrix} \qquad \textbf{(6)}$$

$$\mathbf{Z}_0 = \mathbf{Z}\cdot\boldsymbol{\gamma}^{-\mathbf{T}} = \mathbf{Y}^{-1}\cdot\boldsymbol{\gamma}^{\mathbf{T}} = \boldsymbol{\gamma}^{-1}\cdot\mathbf{Z} = \boldsymbol{\gamma}\cdot\mathbf{Y}^{-1} \qquad \textbf{(7)}$$

$$\mathbf{ZY} = \boldsymbol{\gamma}^2 = (-\boldsymbol{\gamma})^2 = (\mathbf{R} + j\omega\mathbf{L})\cdot(\mathbf{G} + j\omega\mathbf{C}) \qquad \textbf{(8)}$$

where $\mathbf{Z}_0$ is characteristic impedance matrix, $\boldsymbol{\gamma}$ is propagation constant matrix for the segment.

A complete cable can be treated as a cascade of segments. This is for mathematical convenience and practical cable structure. By modeling a complete cable loop as a cascade of segments, the input-output transfer relation for the cable is then:

$$\begin{bmatrix}\mathbf{V}(0)\\ \mathbf{I}(0)\end{bmatrix} = \boldsymbol{\Phi}_1\cdot\boldsymbol{\Phi}_2\ldots\cdot\boldsymbol{\Phi}_N\cdot\begin{bmatrix}\mathbf{V}(d)\\ \mathbf{I}(d)\end{bmatrix} = \boldsymbol{\Phi}\cdot\begin{bmatrix}\mathbf{V}(d)\\ \mathbf{I}(d)\end{bmatrix} \qquad \textbf{(9)}$$

where $\boldsymbol{\Phi}_i$ describes the input-output transfer relationship for one segment, and N is the total number of segments under consideration. Again, overall $\boldsymbol{\Phi}$ can be written as the **A, B, C, and D** matrix:

$$\mathbf{\Phi} = \begin{bmatrix} \mathbf{A} & \mathbf{B} \\ \mathbf{C} & \mathbf{D} \end{bmatrix} \tag{10}$$

Once $\mathbf{\Phi}$ is obtained, it is easy to obtain the MIMO channel transfer function as in the sequel.

2) MIMO Channel Transfer Function

To calculate the MIMO channel transfer function, an input-output voltage transfer function needs to be calculated first. The input-output voltage matrix transfer function for a cable is defined as $\mathbf{T}$ in $\mathbf{V}(d) = \mathbf{T} \cdot \mathbf{V}(0)$, where $\mathbf{V}(0)$ is the input voltage vector to the cable, and $\mathbf{V}(d)$ is the output voltage vector of the cable. The output voltage is related to output current by load admittance matrix $\mathbf{Y}_L$, $\mathbf{I}(d) = \mathbf{Y}_L \cdot \mathbf{V}(d)$. Using the $\mathbf{Y}_L$ and $\mathbf{\Phi}$ in (16), the input to output voltage matrix transfer function $\mathbf{T}$ can be computed as:

$$\mathbf{T} = \left(\mathbf{A} + \mathbf{B}\mathbf{Y}_L\right)^{-1} \tag{11}$$

This formula uses the admittance matrix instead of the impedance matrix because the impedance matrix does not exist under differential load. To get a voltage transfer function between a source and a load, a voltage divider between the source admittance and the input admittance to the cable needs to be considered. The input impedance is defined by: $\mathbf{I}(0) = \mathbf{Y}_1 \cdot \mathbf{V}(0)$, where $\mathbf{I}(0)$ is an input current vector to cable, $\mathbf{Y}_1$ is the input admittance matrix to cable. The formula for the input admittance is given by:

$$\boldsymbol{Y}_1 = \left(\boldsymbol{C} + \boldsymbol{D} \cdot \boldsymbol{Y}_L\right) \cdot \left(\boldsymbol{A} + \boldsymbol{B} \cdot \boldsymbol{Y}_L\right)^{-1} \tag{12}$$

The transfer function $\mathbf{H}(f)$ between an input vector voltage supply $\mathbf{V}_S$ (with a finite internal impedance matrix $\mathbf{Z}_S$) and the output voltage $\mathbf{V}_L$, $\mathbf{V}_L = \mathbf{V}(d)$, can be calculated by considering $\mathbf{Y}_S$, $\mathbf{Y}_1$ and $\mathbf{T}$:

$$\mathbf{H} = \mathbf{T} \cdot \left(\mathbf{Y}_1 + \mathbf{Y}_S\right)^{-1} \cdot \mathbf{Y}_S \tag{13}$$

This formula generates $\mathbf{H}$ as in MIMO channel transfer function $\mathbf{Y} = \mathbf{H}\mathbf{X} + \mathbf{N}$ if the input and output are voltage vectors. For a system with $2N$ conductor wires, when one wire is chosen as a common reference, this method produces a $(2N-1) \times (2N-1)$ MIMO channel. The channel derived in

this way is referred to as a *common mode MIMO channel*. The MIMO channel model works for any source and load admittance ($\mathbf{Y}_S$ and $\mathbf{Y}_L$) (or impedance $\mathbf{Z}_S$ and $\mathbf{Z}_L$) (see Fig. 3(a).) An interesting source-load configuration for this mode is matrix-impedance matching, which is conceptually similar to the single-line case. For the matrix-impedance matching, the load and source impedance matrix can be chosen as:

$\mathbf{Z}_L = \mathbf{Z}_0$, Load matches to the matrix characteristic impedance, or

$\mathbf{Z}_s = \mathbf{Z}_0$, Source matches to the matrix characteristic impedance. (typically source matching is only of interest when the cable is used bi-directionally and so the terminating impedance may be instead a source impedance or near-side impedance through some kind of hybrid circuit)

These matching matrices are particularly meaningful when $\mathbf{Z}_0$ is independent of cable position, as for perfect "quad" cables when neighboring quads are neglected[1]. For such cable, the load matrix matching completely removes the well-known ripples in NEXT vs. frequency curves. In general, $\mathbf{Z}_L$ and $\mathbf{Z}_s$ in these formulas depend on frequency. However, for real cable systems, $\mathbf{Z}_0$ is almost pure resistive above a few hundred kilohertz, so it is easy to design matrix impedance matching at frequency above a few hundred kilohertz. For twisted-pair cable, because $\mathbf{Z}_0$ is position dependent, $\mathbf{Z}_L = \mathbf{Z}_0$ or $\mathbf{Z}_s = \mathbf{Z}_0$ only ensures the load or source matching for a particular cable position, but not for whole cable. In general, the load matrix matching cannot completely remove ripples in NEXT vs. frequency curves as it does for "quad" cable. For both "quad" cable and twisted pair cable, a simpler load-source configuration is to choose $\mathbf{Z}_L$ and $\mathbf{Z}_s$ to be diagonal matrix. For example, for category 3 twisted-pair American telephone lines, diagonal elements of $\mathbf{Z}_L$ and $\mathbf{Z}_s$ can be chosen as 100 Ohms. Such diagonal matching does not correspond to differential termination of each line in its own characteristic differential resistive impedance. Simulations show that the common-mode MIMO channel generated by this simpler load-source configuration is similar to that of the more sophisticated matrix-matching configuration.

The common model MIMO channel is intuitively the default MIMO channel for a binder cable;

[1] "quad" cable is used in France, Germany, and other countries

but a practical communication system that uses such channel might be complicated to implement.

A simpler MIMO model for the binder cable exists. The model is based on differential loads, where sources and loads are individually applied to each pair of conductor wires. In this configuration, FEXT can be defined between pairs and a direct transfer function can be defined for each pair. For a cable system with N pairs, 2N wires, a $N \times N$ channel matrix can be defined for such source-load configuration. In the channel matrix, the direct transfer functions for pairs are on diagonal positions and FEXT is on off-diagonal positions. The channel derived in this way is referred to as a *simplified differential model MIMO channel*. For four conductor wires forming two differential pairs as in Fig. 3(b), the differential model MIMO channel matrix $\mathbf{H}_{sd}$ is:

$$\mathbf{H}_{sd} = \begin{bmatrix} T_1 & FEXT_{12} \\ FEXT_{21} & T_2 \end{bmatrix} \tag{14}$$

In practice, implementing an $N \times N$ differential mode MIMO system is less complicated than implementing a $(2N-1)\times(2N-1)$ common-mode MIMO system. The tradeoff is that the system formed by $2N$ conductor wires has higher channel capacity if the system is modeled as a $(2N-1)\times(2N-1)$ channel rather than an $N \times N$ channel [1]- [2].

Since the source-load voltage relation is given by matrix transfer function **H**, FEXT as well as NEXT and line transfer functions can be calculated from **H** under differential loads and sources.

3) Computation of Scalar Line and Crosstalk Functions with Scalar Sources and Differential Loads

Fig. 4 illustrates a typical situation where excitations are scalar voltages and terminations and sources are differential for two lines where Y_p is the admittance of any load placed across each and every pair, and other quantities are defined by the equations at the bottom of Fig. 4. $\mathbf{Y}_P$ is a 2×2 admittance matrix specified in the figure for the 2 currents in wires 2 and 3. The known admittance matrix $\mathbf{Y}_1$ (defined in Fig. 4) can be used to calculate all scalar transfer functions. From the two basic circuit equations

$$-\mathbf{Y}_P \cdot \mathbf{V}_P = \mathbf{Y}_{22} \cdot \mathbf{V}_P + \mathbf{Y}_{21} \cdot V_1(1) \tag{15}$$

$$I_1(1) = \mathbf{Y}_{21}^T \cdot \mathbf{V}_P + Y_{11} \cdot V_1(1) \tag{16}$$

The relation between in the input current and voltage is then

$$I_1(1) = \underbrace{\left[Y_{11} - \mathbf{Y}_{21}^T \cdot \left(\mathbf{Y}_P + \mathbf{Y}_{22}\right)^{-1} \cdot \mathbf{Y}_{21}\right]}_{y_1} \cdot V_1(1) \quad \textbf{(17)}$$

For a differential source where all use the same impedance, then $Y_P = \begin{bmatrix} \frac{1}{R_S} & -\frac{1}{R_S} \\ -\frac{1}{R_S} & \frac{1}{R_S} \end{bmatrix}$, which is singular. The scalar source voltage to its network input voltage relation is

$$V_S(1) = R_S \cdot I_1(1) + V_1(1) = \left[1 + R_S \cdot y_1\right] \cdot V_1(1) \quad \text{or} \quad \textbf{(18)}$$

$$V_1(1) = \frac{V_S(1)}{1 + R_S \cdot y_1} \quad \textbf{(19)}$$

From (15), one obtains

$$\mathbf{V}_P = -\left(\mathbf{Y}_P + \mathbf{Y}_{22}\right)^{-1} \cdot \mathbf{Y}_{21} \cdot V_1(1) \quad \textbf{(20)}$$

$$\text{Then } H_{NEXT} = \frac{V_1(3) - V_1(2)}{V_S(1)} = \begin{bmatrix} 1 & -1 \end{bmatrix} \cdot \frac{\left(\mathbf{Y}_P + \mathbf{Y}_{22}\right)^{-1} \cdot \mathbf{Y}_{21}}{1 + R_S \cdot y_1} \quad \textbf{(21)}$$

$$\text{and } H_{FEXT} = \frac{V_2(3) - V_2(2)}{V_S(1)} = \begin{bmatrix} 1 & -1 & 0 \end{bmatrix} \cdot \frac{\mathbf{T}}{1 + R_S \cdot y_1} \cdot \begin{bmatrix} \left(\mathbf{Y}_P + \mathbf{Y}_{22}\right)^{-1} \cdot \mathbf{Y}_{21} \\ 1 \end{bmatrix} \quad \textbf{(22)}$$

and the main source to load transfer function is

$$H = \frac{V_2(1)}{V_S(1)} = \begin{bmatrix} 0 & 0 & 1 \end{bmatrix} \cdot \frac{\mathbf{T}}{1 + R_S \cdot y_1} \cdot \begin{bmatrix} \left(\mathbf{Y}_P + \mathbf{Y}_{22}\right)^{-1} \cdot \mathbf{Y}_{21} \\ 1 \end{bmatrix} \quad \textbf{(22)}$$

The other 3 NEXT and 3 FEXT transfer functions can be computed re-indexing the wires and repeating the procedure. Equations (15) and (18)-(20) are valid for any number of lines, in which case the quantities $\mathbf{V}_P$, $\mathbf{I}_P$, $\mathbf{Y}_P$, $\mathbf{Y}_{22}$, and $\mathbf{Y}_{21}$ become $(2n-2)$-dimensional. The leading vectors on the right-hand sides of equations (21) and (22) have the two non-zero entries +1 and -1 in the positions of the line into which the crosstalk is being computed. The leading vector in (22) has all zeros except a 1 in the last (right most) position.

These methods to extract information for differential loads from a common-mode MIMO channel matrix can be applied not only to traditional differential excitation, but also to unconventional differential excitations. There are interesting relations among these excitations.

4) Relation to Traditional Models Involving Differential Excitations and "Phantom" Components

Fig. 5 below shows 3 views of the same 2-twisted-pair cable:

(1) description with all voltages referenced to an external reference (e.g., earth ground) (top)

(2) traditional "symmetric" description using differential excitations and phantoms (left)

(3) asymmetric description of this section that allows direct matrix RLCG models (right) – some of the direct transfers are between the wires of different twisted pair, which are sometimes called "split-pair" transfers.

The relationship between the models is listed in the figure. The 3 voltages of the traditional symmetric model can be related (input or output) to the 3 voltages of the asymmetric model. The symmetric model includes a 3rd voltage ΔV_p that is often colloquially called a ``phantom'' signal (this name is unfortunate because this voltage exists and can be very real in its effects). The voltage with respect to earth ground is not modeled in either symmetric or asymmetric approaches.

Any transfer functions involving differential and/or phantom signals in traditional modeling can always be directly related to transfer functions based on asymmetric voltages and vice versa (table 1). The two are completely equivalent, and no extra information appears in one with respect to the other (in infinite precision measurement of parameters – some could be easier to measure than others). A 4th voltage occurs at the top and would represent a possible transmission mode with respect to earth ground. However, this common is missing in exactly the same way in both of the lower models (and is not used in present DSL transmission systems).

Special case of zeroed phantom(s):

Setting the center taps of the two differential source or load transformers equal corresponds to zeroing the phantom.[1] Then $\Delta V_p = 0 \Rightarrow V_3 + V_2 = V_1$ (remembering that V_2 and V_3 are not differential voltages and referenced to one of the 4 wires), and a 2nd potential model of transmission is silenced by the constraint, leaving only two possible modes, the obvious differential modes. If these two center taps are not equal, a 3rd mode of transmission may be either abused or exploited.

[1] The most common way of zeroing the phantom is to ground both center taps, and thus they are equal.

The above discussions show that for a cable system with given source-load configuration, if the channel matrix **H** is known, the magnitude and the phase of individual NEXT, FEXT, split-pair and phantom transfers can all be calculated. Additionally, for a given source-load configuration, if **RLCG** matrices are known for each segment, then the channel matrix **H** can be obtained. Thus, to complete the model, methods to find **RLCG** matrices for each cable segment are needed.

*5) Calculations of **RLCG***

For given cable geometry, two methods can be used to obtain per unit length **RLCG** matrix. One method is based on analytical approach using basic electromagnetic theory; another method is based on extracting matrix elements from measured data. Calculation of **RLCG** directly from the basic electromagnetic principle inevitably involves some approximations. Established methods with various levels of approximation can be found in [4], [11], [12]. One disadvantage of the calculation approach is that it requires knowing $\mu, \varepsilon_r, \sigma$ of dielectric filling material of cables and the conductivity of metal conductors. These values maybe not easy to obtain or to estimate. The approach based on extracting **RLCG** from measurement overcomes such difficulties [10]. However, there are drawbacks of this approach too. Typically, the frequency-dependent characteristics of a single pair are measured for an isolated twisted pair. In other words, the measured twisted pairs were not in a cable binder, so that the measured values are not completely suitable for actual twisted pairs inside a cable binder; therefore, this approach only works as an alternative approximation. In actual simulations, both methods can be implemented, when some measured data are available, one method maybe favored over another. Regardless the differences of these two methods, both depend on knowing cable geometric parameters. For this cable-geometry dependence, the proposed binder MIMO model includes the following cable geometric models.

B. Cable Geometric Model

To calculate the **R, L, C, G** matrices, the actual cable geometry needs to be considered. Two types of geometric configurations are discussed in this section: "quad" cables and twisted-pair cables. It can be shown theoretically [8], [13], and confirmed by simulations in this work, that cable imperfections are

important to characterize the channel. So for each type of cable, geometric modeling also contains cable imperfection modeling.

1) Geometric Modeling of Quad Cable

Ideal "quad" cable has nice symmetric properties, the four wires in a quad are parallel to each other, and the centers of 4 wires form a square. The symmetry ensures that crosstalk for quad cable under normal differential excitation, where source and load are setup over one diagonal pair and crosstalk is measured over the other diagonal pair, is zero. In real imperfect quad cables, the centers of the 4 wires cannot form a perfect square. Thus, the expected symmetry is imperfect. Quads in a binder rotate along the cable. The rotation does not affect crosstalk characteristics among 4 conductor wires in the same quad, but does reduce crosstalk between different quads, much like twisting in twisted pair reduces crosstalk between twisted pairs. A description of the geometry of a basic quad cable requires only the positions of 4 conductor centers and the conductor radii.

2) Geometric Modeling of the Twisted Pair Cable

Geometric modeling of twisted pair includes twisting description and imperfection description. To describe twisting of a pair, the trajectory of the pair center as well as the relative rotations of two wires against pair center are needed. Different levels of approximation have been proposed in past to describe twisting [5]-[6], [14]. For simulation purposes in this work, the single-pair discrete-rotation model [14] is extended to multiple-pair discrete rotation [13], where every pair in a twisted cable is modeled as discretely rotating. The modeling of binder-MIMO imperfection mainly considers three types of cable imperfection: pair-center adjustments, twist-rate adjustments and non-twisting segment at cable head or tail.

a) Type I Imperfection in Twisted Pair Cable: Pair Center Adjustments

The pair-center variation denotes the situation in which the pair centers deviate from the expected position. For ideal parallel layout of twisted pairs, the pair centers of any two pairs form two parallel straight lines, and the distance between the two wire centers in each twisted pair is fixed. This ideal cable is called "perfect twisted pair cable in this work." It can be analytically proved that

electromagnetic couplings between perfect twisted pairs almost entirely cancel under normal differential excitation [13]. In reality, because manufacturing procedures are not perfect and twisted pairs are densely packed inside cables, pair centers cannot form straight parallel lines and thus, pair center separation varies.

Let $pc(i,z)$ denote the pair center of pair i along the cable of length z.

$$pc(i,z) = \overline{pc}(i,z) + \Delta pc(i,z) \quad \textbf{(23)}$$

where i is an index for each pair in a twisted pair cable, $\overline{pc}(i,z)$ is the expected pair center position for pair i at the cable of length z and $\Delta pc(i,z)$ is the deviation from the expected position. For non-parallel wires within the cable, $\overline{pc}(i,z)$ can be described by known parameters. In this work, two pair-center adjustment methods are introduced: a random adjustment method and a sinusoidal adjustment method. In the case of the random adjustment,

$$\Delta pc(i,z) = \alpha(i,z) \cdot \overline{pc}_0(i) \quad \textbf{(24)}$$

where $\alpha(i,z)$ is a random function of z, z denotes the length from cable head or tail. For a practical twisted pair cable structure, simulations shows that the value of $\alpha(i,z)$ is most likely in the range of [0, 0.15]; $\overline{pc}_0(i)$ is the average of the pair center position. For the sinusoidal adjustment,

$$\Delta pc(i,z) = \alpha_i \sin(k_i \cdot z) \cdot \overline{pc_0}(i) \quad \textbf{(25)}$$

where α_i is a constant for a pair, k_i denotes space frequency. In the case of a single pair discrete rotation, k_i is a reciprocal of the twist rate of the pair. For two pairs or multi-pair discrete-rotation model, k_i can be obtained from the geometric cable structure. Simulations show that $0 < \alpha_i < 0.2$ works for many practical twisted-pair cable structures. A few more sophisticated pair-center adjustment options have been investigated to include the "squeezing" effect from the neighboring pairs, however, their improvements were negligible and not further considered here. The net effect of pair-center variation is that such variation breaks the electromagnetic-coupling cancellation mechanism inside a length of the basic cycle for perfect twisted pairs and thereby increases the electromagnetic coupling between pairs. Equivalently, the pair-center variation then increases FEXT to levels that are consistent

with those measured in practice. However, pair-center variation alone is not enough to explain the measured NEXT, which necessitates another type of adjustment, called 'a twist rate non-uniformity adjustment'.

b) Type II Imperfection in Twisted Pair Cable: Twist Rate Non-Uniformity Adjustments

NEXT is proportional to the constructive reflection when the electromagnetic wave travels along a cable. For a twisted-pair cable system with a periodic nature of cable geometry, the effective averaging over a basic period of the twisting causes a uniform appearance of **RLCG** matrices. Accordingly, matrix characteristic impedance is uniform. This implies that that although there can be minor reflections of electromagnetic waves inside a section of the cable corresponding to one period, there is not much reflection between such periods. In a real cable, the uniformity of cable is not guaranteed. Consequently larger section-to-section reflections are often created and lead to the high NEXT levels usually observed in measurements. There are a few possible reasons for this "uniformity break": the first reason is the existence of the neighboring pairs. However, simulation results suggest that neighboring pairs do not induce enough reflection. A more likely reason is the twist-rate non-uniformity. To model the twist-rate non-uniformity, a twist-rate distribution function is defined. Let $P_{tr}(tr)$ be a probabilistic distribution of a twist rate tr, and $P'_{tr}(tr)$ be an ideal probabilistic distribution of a twist rate. The ideal twist-rate distribution is a delta function, $P'_{tr}(tr) = \delta(tr - \overline{tr})$, where $\overline{tr}$ is an expected twisted rate by the cable manufacturer. In a real cable, the twist rate has a non-delta distribution function centered at the expected twist rate. Uniform and Rayleigh distributions for a twist rate are proposed and used in simulations in this work. For the uniform distribution, the following $P_{tr}(tr)$ can be used:

$$P_{tr}(tr) = 1/2a, tr \in [\overline{tr} - a, \overline{tr} + a] \quad \textbf{(26)}$$

For practical purposes, $a < 0.2 \cdot \overline{tr}$ can be chosen. For the Rayleigh distribution, $P_{tr}(tr)$ is given by:

$$P_{tr}(tr) = \frac{(tr) \cdot \exp(-(tr)^2 / (2 \cdot (\overline{tr})^2)}{(\overline{tr})^2} \quad , \quad \textbf{(27)}$$

which has the largest value when $tr = \overline{tr}$. To simulate practical systems, too short or too long twist rate can be excluded. After selecting a twist-rate distribution function, the simulation software randomly picks twist rates according to the distribution function and arranges them along the cable until the complete cable length is reached. Partial twists may be needed at the end of the cable if full twists cannot exactly match the targeted cable length.

c) Type III Imperfection in Twisted Pair Cable, Non-twisting Cable Head or Tail

In real cables, non-twisting tail and head sections may occur at connection points (ends of the cable). Even though the length of the cable tail or head section might be only a few centimeters, a very short length compared to a full cable length, simulations show that such short non-twisted sections may significantly affect the overall crosstalk level for the whole cable. This is because crosstalk from these non-twisting tail and head sections do not experience any cancellation.

Based on circuit theory and cable geometry descriptions, the binder MIMO model can calculate channel transfer functions for a binder or cable from basic system parameters, a few examples are presented in next section.

III. Channel Characteristics and Numerical Examples

This section contains results for a few numerical examples and discusses general qualitative characteristics for binder channels. These results are also compared with analytical predictions and measured data. The main purpose of these examples is to verify the model. Since measured data are typically only available for differential excitations, this section focuses on examining the simulation results for differential excitation.

Due to their relative simplicities, crosstalk properties for "quad" cables are present first. Here, crosstalk is shown to be completely cancelled for the ideal "quad" cable under normal differential excitation. Then, crosstalk properties for twisted-pair cables are presented, with a focus on the effect of cable imperfections. The data shows that crosstalk is almost entirely cancelled for ideal twisted-pair cable, but in real cable, the pair-center variation and the twist-rate variation can greatly affect the crosstalk level. The simulations also show that cable imperfections have a substantial impact on

crosstalk yet have a relatively small impact on the direct transfer function for a twisted pair. Results on how crosstalks depend on cable length will then follow. Last, simulation results are shown to match well with measured data.

A. Crosstalk for both Perfect and Imperfect Quad Cables

For a perfect basic "quad" cable, the centers of 4 wires form a square. The distances between the 4 wires are denoted as D-D-D-D. For the cable, normal differential excitation is to excite over a pair of diagonal wires, and crosstalk is measured over the other pair of diagonal wires; split-pair differential excitation excites two wires on the same side of a quad and crosstalk is measured over other two wires. Fig. 6(a) shows the crosstalk of the 2-meter long perfect basic quad cable. Clearly, crosstalk under the normal differential excitation is completely cancelled. It can be shown analytically that the cancellation is caused by the perfect geometric symmetry of quad cables. The figure also shows that the crosstalk under the split-pair differential excitation is not cancelled. If the perfect symmetry is broken, the crosstalk cancellation mechanism of the diagonally excited quad is degraded. Fig. 6(b) shows crosstalk for a quad where the centers of 4 wires are slightly deviated from a perfect square. The distances of 4 wires are D-1.02D-D-1.02D (2% deviation from a square). Even with such small asymmetry, the significant crosstalk under the normal differential excitation is clearly observed. More simulations show that, for many practical cables, 2% deviation from a square works as a good approximation to compute crosstalk levels that match measurements.

B. Effects of Cable Imperfection on Crosstalk For Twisted Pair Cable

Fig. 7 shows the effect of cable imperfections on FEXT and NEXT as well as upon the direct transfer function between two twisted pairs under normal differential excitation. Here, the normal differential excitation is referred to as exciting two wires in the same twisted pair, and crosstalk is measured for another twisted pair. The length of the cable is 274 meters, and the type of the cable is 24 American wire gauge (AWG). The twist rate for one pair is 4.0inch (≈ 10.1centimeter) and for another pair, it is 6.2 inch (≈ 15.7centimeter). A parallel layout is used for the simulation, and the expected distance between pair centers is 1.7mm. The figure shows results for 4 different scenarios: perfect

twisting, with type III imperfection only (untwisted cable head and tail), with type III and type I imperfection (pair center adjustment), with type III, I and II (twist rate adjustment). Parameters used in describing imperfections are: the 10% random pair-center variation, 3 cm untwisted cable head and tail, and the uniform twist-rate distribution, where $P_{tr}(tr) = 1/2a, tr \in [\overline{tr} - a, \overline{tr} + a]$, $a = 0.15 \cdot \overline{tr}$. A few outstanding characteristics can be observed in this figure; First, without cable imperfection, both FEXT and NEXT are very small, which illustrates that the crosstalk is mostly cancelled for perfect twisted pairs, but this cancellation is not as complete as for the earlier example of the "quad" cables. This conclusion is analytically proved in [13]. Second, imperfections have a big impact on FEXT and NEXT levels; in particular, the twist-rate variation causes the NEXT to exhibit irregular patterns of notches and peaks over frequency. Third, the direct-pair transfer function is not significantly affected by imperfections. Even though these simulation results are obtained for the specific parameters used in this example, the general trends hold for other parameters. In general, simulation results suggest that, for a twisted pair cable system, cable imperfections have great impact on crosstalk under the normal differential excitation, but small impact for crosstalks under split pair differential excitation [13]. Here, split-pair differential excitation is defined as follows: for two twisted pairs, a source is excited between two wires in different twisted pairs, and crosstalk is measured over the remaining two wires. Additionally, if non-differential excitation is used, such as source and load are matrix matched to cable binder, cable imperfections are shown to have small impact to crosstalk and line transfer functions [13].

C. Partial Twist Effect and Crosstalks vs. Cable Length

Fig. 8(a) shows an example how NEXT and FEXT, as well as the direct pair transfer function, vary under the normal differential excitation when the cable length changes. Twist rates are 2.0 inch ($\approx 0.051m$) and 3.9 inch ($\approx 0.099m$) for each of two twisted pairs. The figure plots the average direct transfer function, NEXT and FEXT over the frequency range of 0-20 MHz. In Fig. 8(a), cable length changes from 274 to 274.2 meter. As expected, the direct transfer function remains almost constant when the cable length has such small variations. However, both NEXT and FEXT are very sensitive to the cable length variations, even though the variations are smaller than twist rates. The effect, here

named the "Partial Twist Effect", has been observed in measurements [7], [15] and theoretically analyzed in [7], [13]. The partial-twist effect has a considerable impact on the signal-to-noise ratio (S/N) for twisted pairs under the usual differential excitation. For differential excitation, typically FEXT dominates other noises. An approximation formula for S/N is: $S/N = Signal/(FEXT + OtherNoises) \approx Signal/FEXT$. The partial-twist effect implies that S/N can have a few dB variation along a few centimeters in the binder. Furthermore, simulation results suggest that the partial-twist effect happens only under the normal differential excitation but not under split-pair differential excitation. Additionally, simulations show that non-twisted cable head or tail can cause the similar effect. These effects can have interesting practical implications. In practical system design, the length of the cable head, tail or partial twist can be used as "tuning knob" to reduce crosstalk. Using this method, a few dB gain in the signal-noise ratio can be achieved for the normal differential excitation.

Fig. 8(b) shows a related but different effect. It shows how the direct-line transfer function and crosstalk vary with large cable length changes. The simulation uses same parameters as in Fig. 8(a) except that cable length changes from 20 meters to 1200 meters. As can be seen from the figure, the direct transfer function monotonically decreases as the cable length increases, but the crosstalk does not decrease monotonically. The non-monotonic decrease of crosstalk is not all caused by the partial-twist effect. Because if the cable length is carefully chosen such that the partial twist is completely removed, nevertheless, the similar dependency on the cable length is still observed. As a consequence of this effect, S/N can vary by a few dB when the cable length increases. Therefore, a receiver at the near distance from a source might have worse S/N than a receiver at a greater distance with the usual differential excitation.

D. Simulation vs. Measured Data

Fig. 9(a) shows the measured values of the direct transfer function of a pair, NEXT and FEXT between two pairs in a real cable system. The cable consists of 25 twisted pairs (24AWG) of 274 meters length. Fig. 9(b) shows the simulation results with 10% random pair-center adjustment and

uniform twist-rate distribution, $P_{tr}(tr) = 1/2a, tr \in [\overline{tr} - a, \overline{tr} + a]$ where $a = 0.15 \cdot \overline{tr}$ are used. The simulation results depend on the random-number generator (each random output of which of course represents an exactly specific cable). The figure shows the results for one specific random number generator, results that match the measured data well suggesting that this particular random number is a good match to the specific cable imperfection.

The numerical results generated by the simulations in this paper depend on specific sets of cable parameters, and in some cases, random number generators, and these results should be considered as more exploratory than definitive. In addition to above examples, the binder MIMO model has been used to generate power sum for all crosstalk in a cable binder, and simulation results has been compared with empirical results [10]. Results for common mode MIMO channel using matrix match load are reported in [16].

IV. Conclusion

In this paper, binder MIMO channel model is proposed to characterize the physical channels of multi-wire communication systems. The model is flexible in that it can accommodate various kinds of practical cables with different cable geometries, source-load configurations, and different types of cable imperfections. The model can be used not only to calculate NEXT and FEXT when a cable is used under (traditional) differential excitations, but also to calculate a MIMO channel matrix **H** when the system uses MIMO transmission methods. Once the channel matrix **H** is revealed, the achievable data rate of multi-wire communication systems can be calculated**.** The model builds relationship between the channel matrix **H** and the actual physical parameters such as source-load configurations, cable types and geometry parameters; therefore, it can relate the achievable data rate with these parameters and provide helpful insights in real system designs.

References

[1] T. Starr, M. Sorbara, J. M. Cioffi, P. J. Silverman, DSL Advances. Prentice Hall, 2003

[2] G. Ginis, J. M. Cioffi, "Vectored transmission for digital subscriber line systems", *IEEE J. Select. Areas Commun*, VOL. 20, NO. 5, JUNE 2002, pp.1085-1104

[3] T. Starr, J. M. Cioffi, P. J. Silverman, Understanding Digital Subscriber Line Technology. Prentice Hall, 1999

[4] C. R. Paul, Analysis of Multiconductor Transmission lines. New York : Wiley, 1994.

[5] C. R. Paul and J. W. McKnight, "Prediction of crosstalk involving twisted pairs of wires —Part I: A transmission-line model for twisted-wire pairs," *IEEE Trans. Electromagn. Compat.*, vol. 21, pp.92–105, May 1979.

[6] C. R. Paul, Introduction to Electromagnetic Compatibility. Wiley-Interscience, 1992, ch. 10.

[7] C. R. Paul and M. B. Jolly, "Sensitivity of crosstalk in twisted-pair circuits to line twist," *IEEE Trans. Electromagn. Compat.*, vol. 24, pp. 359–364, Aug. 1982.

[8] D. Bellan, S.A. Pignari, G. Spadacini, "Characterisation of crosstalk in terms of mean value and standard deviation", IEE Proc.-Sci. Meas. Technol., Vol. 150, No. 6, Nov 2003 and reference therein.

[9] C. Valenti, "NEXT and FEXT models for twisted-pair north American loop plant", *IEEE J. Select. Areas Commun.*, VOL. 20, NO. 5, JUNE 2002 pp.893-900

[10] J. Cioffi, B. Lee, M. Mohseni, M. H. Brady, K. Seong, Y. Kim, "Evolving channel modeling text for section 5.1 of DSM report", ANSI Contribution T1E1.4/2003-033R2, Aug. 2003

[11] Jeannie Lee, "Modeling and characterization of copper access systems" Ph.D. dissertation, Dept. Elect. Eng., Stanford Univ., Stanford, CA, 2002.

[12] J. A. B. Faria, M. V. G. das Neves, "Analysis of the helical twisted-wire pair running above ground: transfer function evaluation", IEEE Trans. Electromagn. Compat. Vol 45, pp. 449-453, May 2003

[13] Bin Lee, "Binder MIMO Channel" Ph.D. dissertation, Dept. Elect. Eng., Stanford Univ., Stanford, CA, 2004.

[14] M. B. Jolly and C. R. Paul, "Basic EMC technology advancement for C3 systems-crosstalk in twisted-wire circuits," Rome Air Development Center, Griffiss Air Force Base, NY, RADC-TR-82–286, vol. IV C, 1982.

[15] D. Joffe, "End effects on capacitance and inductance measurements in paired cable", ANSI Contribution T1E1.4/2002-238, Nov. 2002 and reference therein.

[16] B. Lee, J. Cioffi, M. Mohseni, "Gigabit DSL", submitted

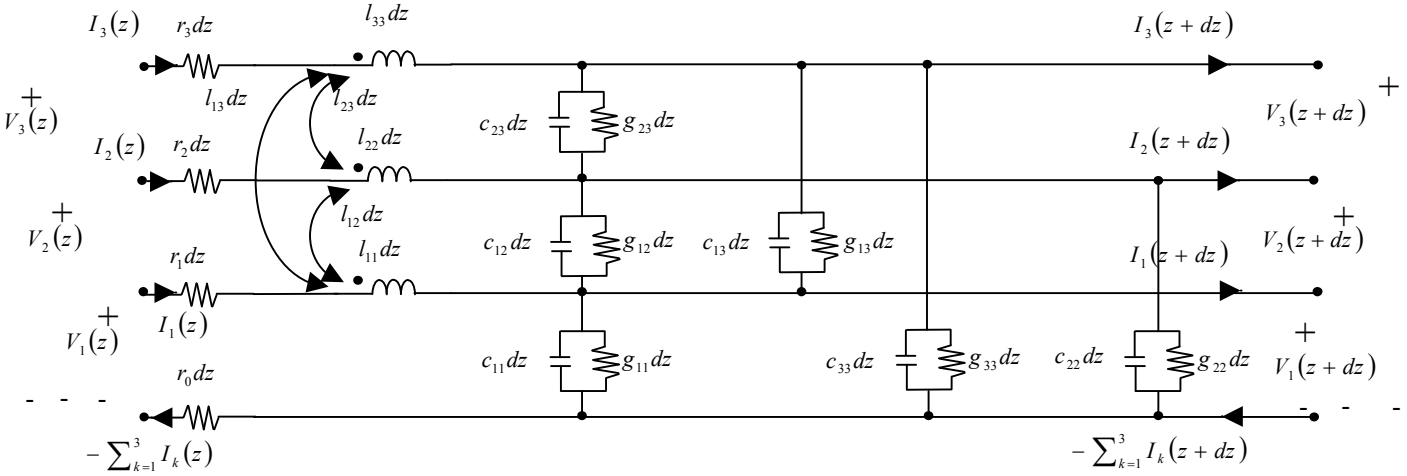

$$\mathbf{R}=\begin{bmatrix} r_0+r_3 & r_0 & r_0 \\ r_0 & r_0+r_2 & r_0 \\ r_0 & r_0 & r_0+r_1 \end{bmatrix} \quad \mathbf{L}=\begin{bmatrix} l_{33} & l_{23} & l_{13} \\ l_{23} & l_{22} & l_{12} \\ l_{13} & l_{12} & l_{11} \end{bmatrix} \quad \mathbf{C}=\begin{bmatrix} c_{13}+c_{23}+c_{33} & -c_{23} & -c_{13} \\ -c_{23} & c_{12}+c_{23}+c_{22} & -c_{12} \\ -c_{13} & -c_{12} & c_{13}+c_{12}+c_{11} \end{bmatrix}$$

$$\mathbf{G}=\begin{bmatrix} g_{13}+g_{23}+g_{33} & -g_{23} & -g_{13} \\ -g_{23} & g_{12}+g_{23}+g_{22} & -g_{12} \\ -g_{13} & -g_{12} & g_{13}+g_{12}+g_{11} \end{bmatrix}$$

Figure 1(a), A segment of cable binder can be described with **R**, **L**, ***C***, **G** and **V**, **I**

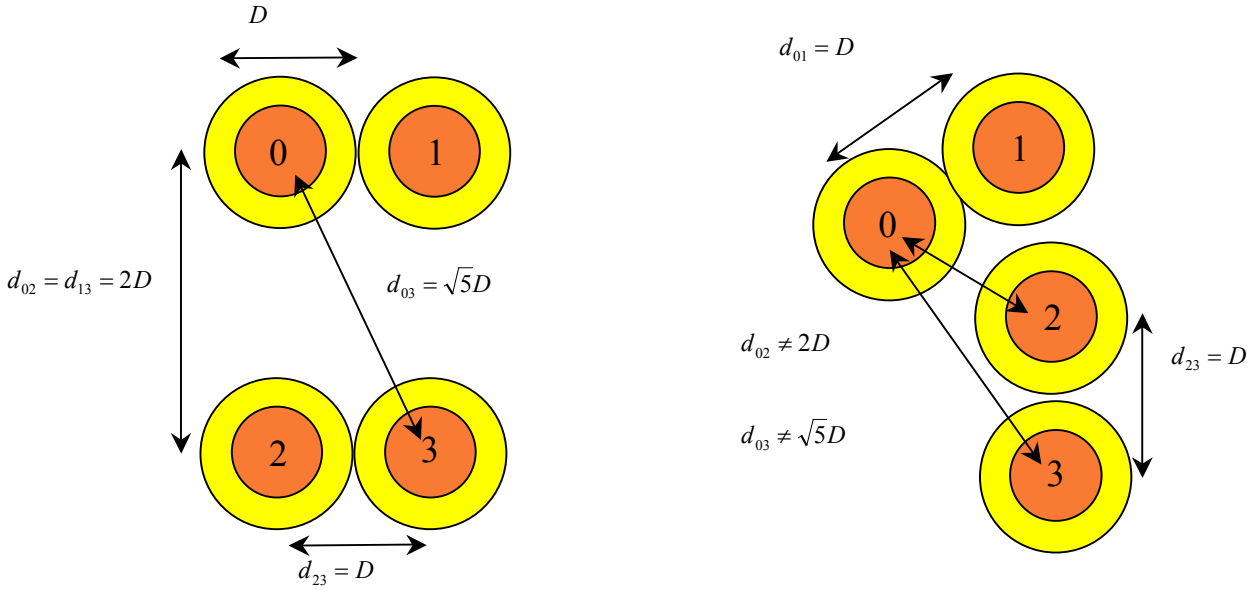

Figure 1 (b), Distance Between Pairs (and thus the **LCG** values) Varies with Twisting

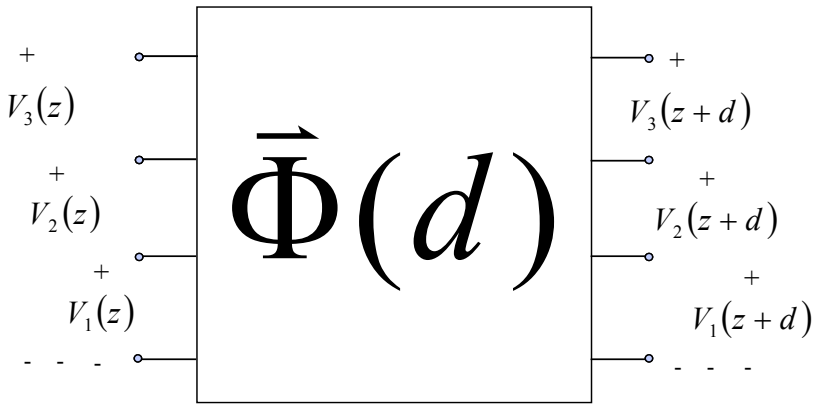

Figure 2, Voltage Input and Output Characteristics of a Cable Segment

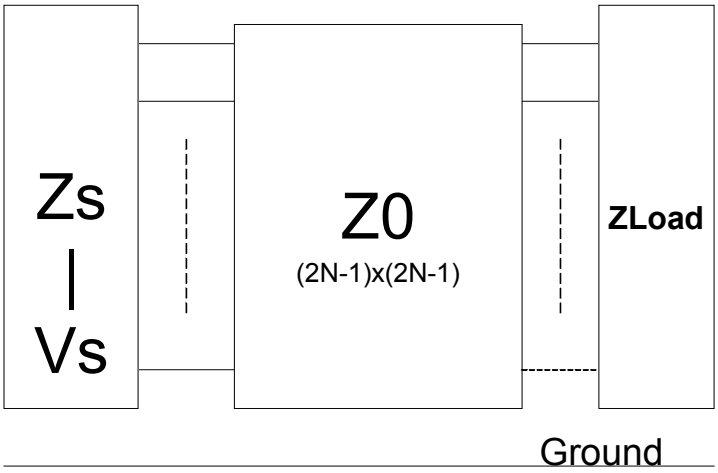

(a) Common Mode MIMO Channel For 2N conductor wires

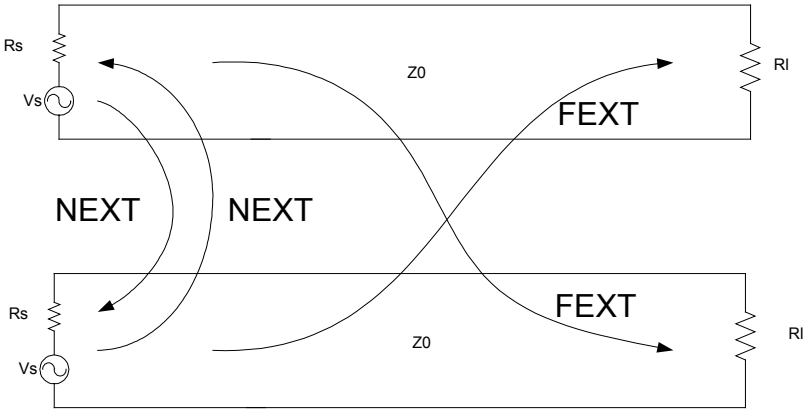

(b) Differential Mode MIMO Channel for 4 conductor wires

Figure 3, Common Mode vs. Differential Mode MIMO Channel

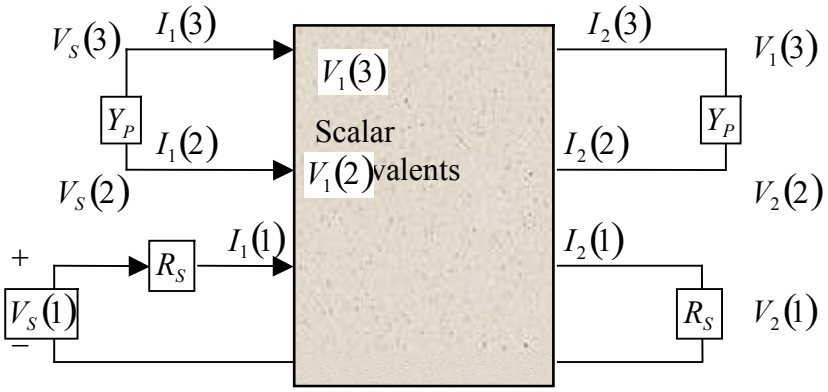

$$-\begin{bmatrix} I_1(3) \\ I_1(2) \end{bmatrix} = \mathbf{Y}_P \cdot \begin{bmatrix} V_1(3) \\ V_1(2) \end{bmatrix} \qquad \mathbf{I}_1 = \begin{bmatrix} -\mathbf{I}_P \\ I_1(1) \end{bmatrix} \qquad \mathbf{V}_1 = \begin{bmatrix} \mathbf{V}_P \\ V_1(1) \end{bmatrix} \qquad \mathbf{I}_1 = \mathbf{Y}_1 \cdot \mathbf{V}_1 \qquad \mathbf{Y}_1 = \begin{bmatrix} \mathbf{Y}_{22} & \mathbf{Y}_{21} \\ \mathbf{Y}_{21}^T & Y_{11} \end{bmatrix}$$

$$-\mathbf{I}_P = \mathbf{Y}_P \cdot \mathbf{V}_P$$

Figure 4, Scalar Sources and Differential Loads

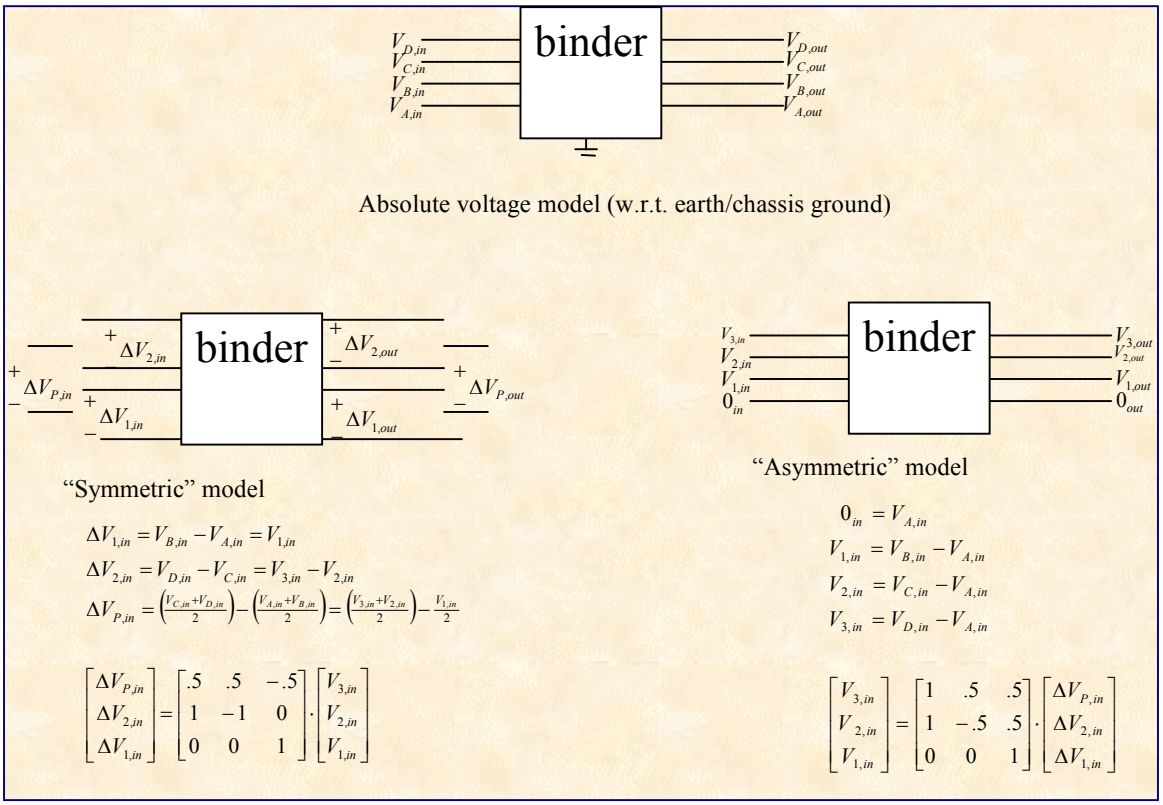

$$\Delta V_{1,in} = V_{B,in} - V_{A,in} = V_{1,in}$$
$$\Delta V_{2,in} = V_{D,in} - V_{C,in} = V_{3,in} - V_{2,in}$$
$$\Delta V_{P,in} = \left(\frac{V_{C,in}+V_{D,in}}{2}\right) - \left(\frac{V_{A,in}+V_{B,in}}{2}\right) = \left(\frac{V_{3,in}+V_{2,in}}{2}\right) - \frac{V_{1,in}}{2}$$

$$\begin{bmatrix} \Delta V_{P,in} \\ \Delta V_{2,in} \\ \Delta V_{1,in} \end{bmatrix} = \begin{bmatrix} .5 & .5 & -.5 \\ 1 & -1 & 0 \\ 0 & 0 & 1 \end{bmatrix} \cdot \begin{bmatrix} V_{3,in} \\ V_{2,in} \\ V_{1,in} \end{bmatrix}$$

$$0_{in} = V_{A,in}$$
$$V_{1,in} = V_{B,in} - V_{A,in}$$
$$V_{2,in} = V_{C,in} - V_{A,in}$$
$$V_{3,in} = V_{D,in} - V_{A,in}$$

$$\begin{bmatrix} V_{3,in} \\ V_{2,in} \\ V_{1,in} \end{bmatrix} = \begin{bmatrix} 1 & .5 & .5 \\ 1 & -.5 & .5 \\ 0 & 0 & 1 \end{bmatrix} \cdot \begin{bmatrix} \Delta V_{P,in} \\ \Delta V_{2,in} \\ \Delta V_{1,in} \end{bmatrix}$$

Figure 5, Equivalence of Traditional Symmetric Model and Asymmetric Model

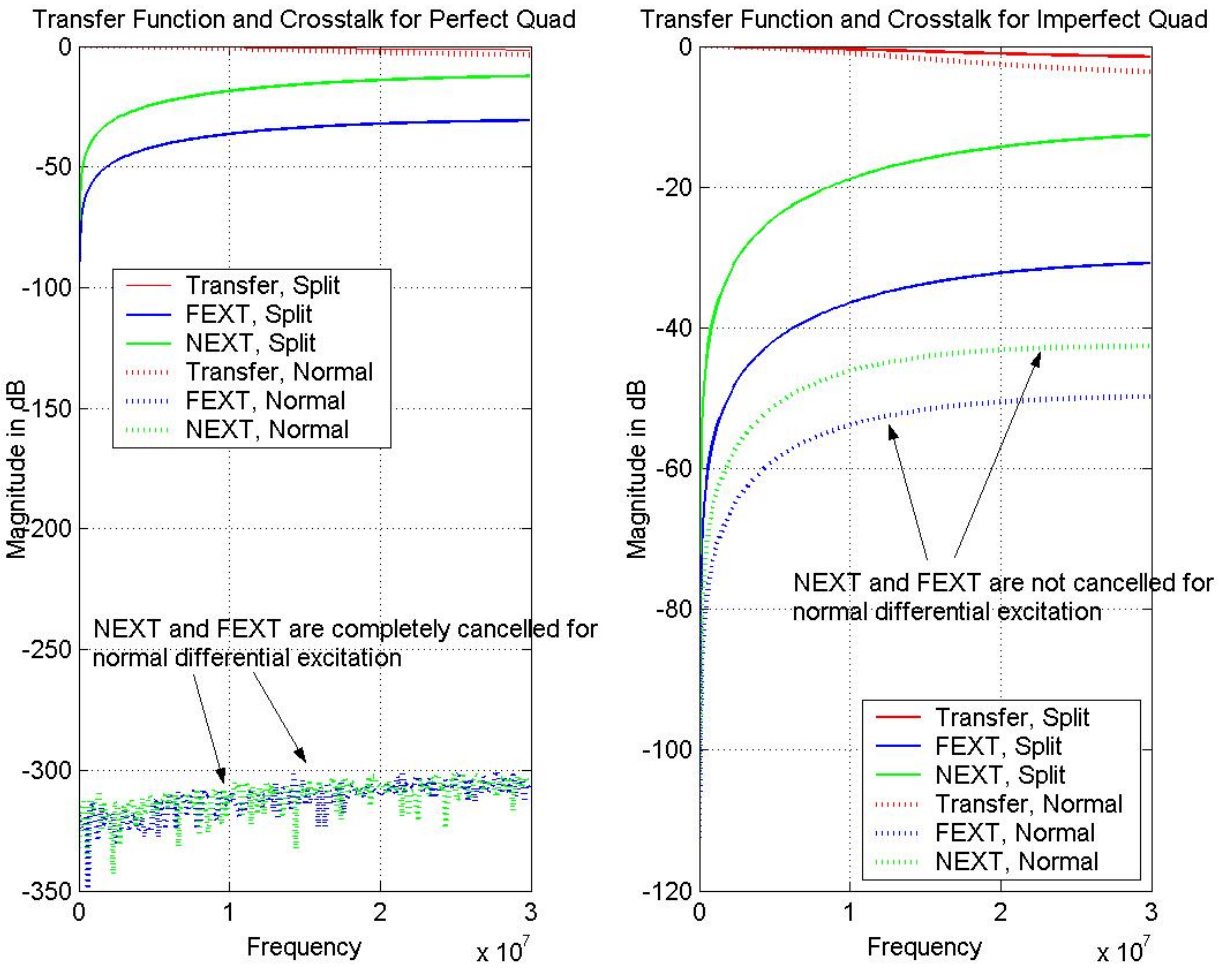

(a) (b)

Figure 6, Crosstalk for 2 Meter Perfect and Imperfect Quad Cable

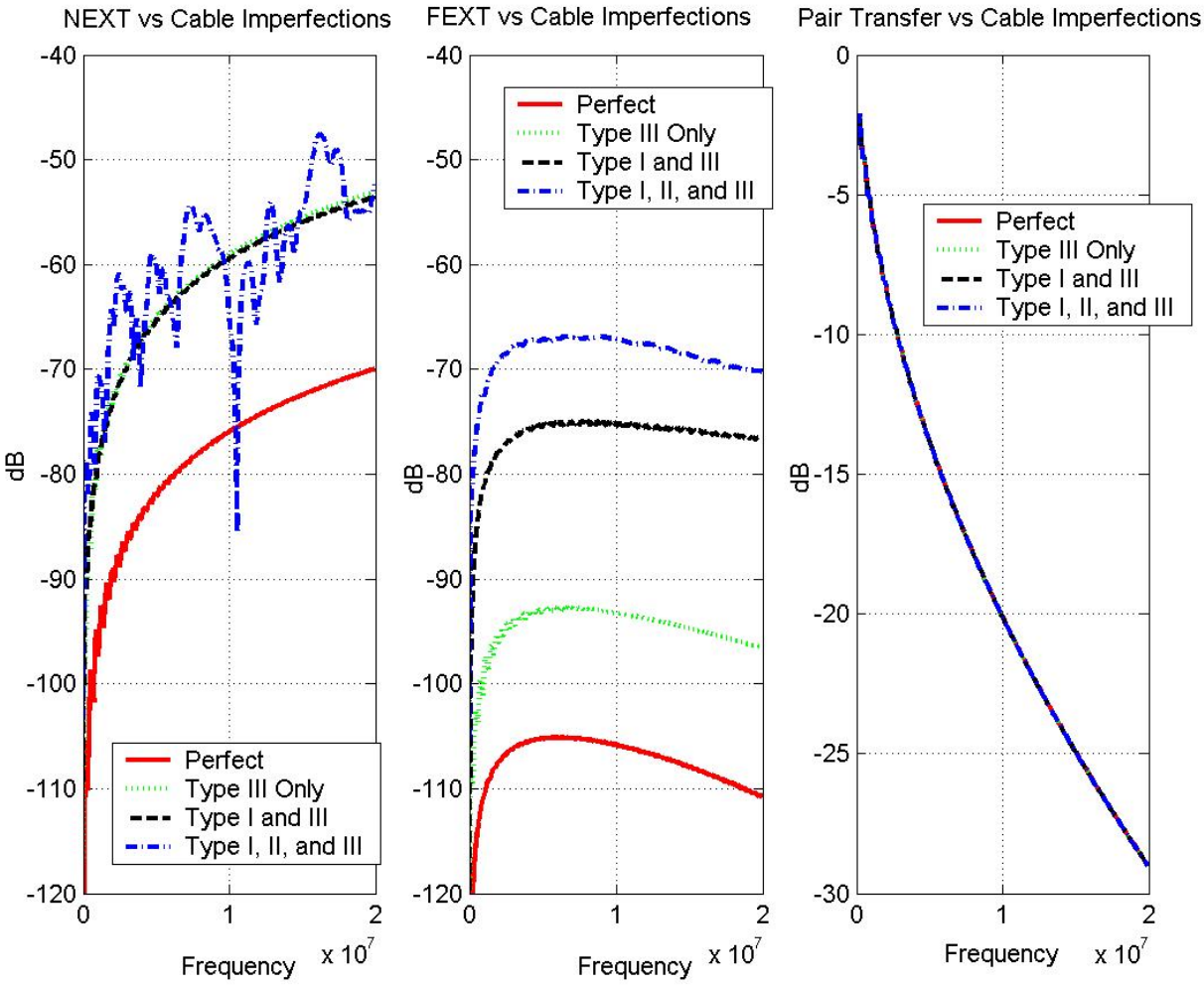

Figure 7, Effect of Cable Imperfection On Crosstalks Under Normal Differential Excitation

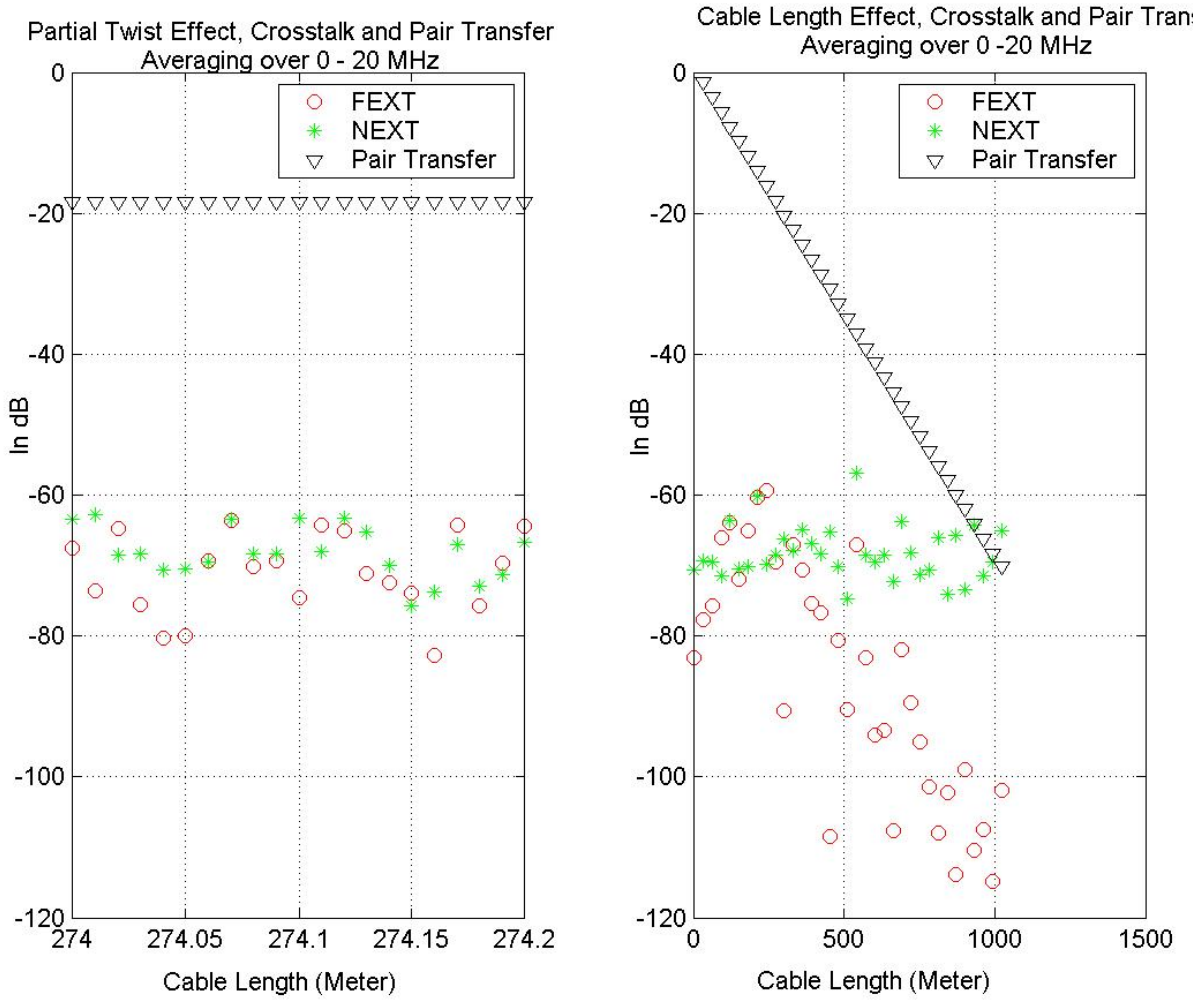

(a) (b)

Figure 8, Crosstalk as Function of Partial Twist and Cable Length

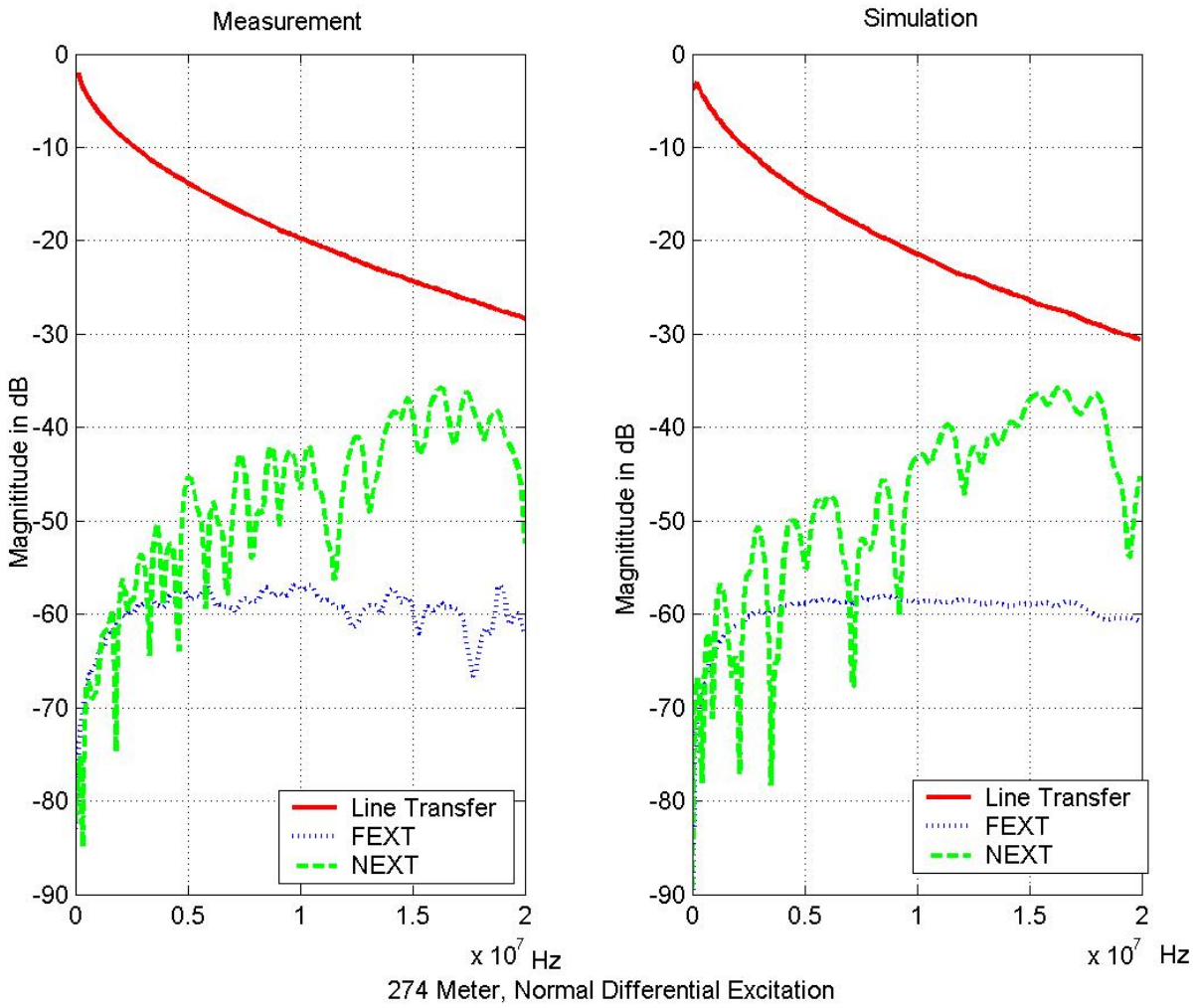

(a) (b)

Figure 9, Simulation vs. Measurement

Table 1
15 Transfer functions of interest for 3x3 Case – G is used for NEXT and H for FEXT
(first subscript is output and second subscript is input)

Label	Symmetric	Asymmetric
Direct transfers	$\frac{\Delta V_{1,out}}{\Delta V_{1,in}}$ $\frac{\Delta V_{2,out}}{\Delta V_{2,in}}$	$\frac{V_{1,out}}{V_{1,in}} = H_{11}$ $\frac{V_{3,out} - V_{2,out}}{V_{3,in} - V_{2,in}} = \frac{H_{32} - H_{22}}{G_{32} - 1}$
FEXTs	$\frac{\Delta V_{2,out}}{\Delta V_{1,in}}$ $\frac{\Delta V_{1,out}}{\Delta V_{2,in}}$	$H_{31} - H_{21}$ $\frac{H_{12}}{G_{32} - 1}$
NEXTs	$\frac{\Delta V_{2,in}}{\Delta V_{1,in}}$ $\frac{\Delta V_{1,in}}{\Delta V_{2,in}}$	G_{21} G_{12}
Phantom FEXTs	$\frac{\Delta V_{2,out}}{\Delta V_{P,in}}$ $\frac{\Delta V_{1,out}}{\Delta V_{P,in}}$ $\frac{\Delta V_{P,out}}{\Delta V_{2,in}}$ $\frac{\Delta V_{P,out}}{\Delta V_{1,in}}$	$\frac{2(H_{31} - H_{21})}{G_{31} + G_{32} - 1}$ $\frac{2(H_{11})}{G_{31} + G_{32} - 1}$ $\frac{H_{32} + H_{22} - H_{12}}{2(G_{32} - 1)}$ $\frac{H_{31} + H_{21} - H_{11}}{2}$
Phantom Direct	$\frac{\Delta V_{P,out}}{\Delta V_{p,in}}$	$\frac{H_{31} + H_{21} - H_{11}}{G_{31} + G_{21} - 1}$
Phantom NEXT	$\frac{\Delta V_{2,in}}{\Delta V_{P,in}}$ $\frac{\Delta V_{1,in}}{\Delta V_{P,in}}$ $\frac{\Delta V_{P,in}}{\Delta V_{2,in}}$ $\frac{\Delta V_{P,in}}{\Delta V_{1,in}}$	$\frac{2(G_{31} - G_{21})}{G_{31} + G_{32} - 1}$ $\frac{2}{G_{31} + G_{32} - 1}$ $\frac{G_{32} + G_{22} - G_{12}}{2(G_{32} - 1)}$ $G_{31} + G_{21} - 1$

Table 1, Results For Symmetric and Asymmetric Mode